Tellus (1989), *41A*, 292–307

Minimal modeling of the extratropical general circulation

By ENDA O'BRIEN, *University of Miami, Rosenstiel School of Marine and Atmospheric Science, Miami, Florida 33149, USA* and LEE E. BRANSCOME, *Environmental Dynamics Research, Inc., 100 Ocean Lane Drive, Suite 305, Miami, Florida 33149, USA*

(Manuscript received 21 April 1988; in final form 6 December 1988)

ABSTRACT

The ability of low-order, two-layer models to reproduce basic features of the mid-latitude general circulation is investigated. Changes in model behavior with increased spectral resolution are examined in detail. Qualitatively correct time-mean heat and momentum balances are achieved in a β-plane channel model which includes the first and third meridional modes. This minimal resolution also reproduces qualitatively realistic surface and upper-level winds and mean meridional circulations. Higher meridional resolution does not result in substantial changes in the latitudinal structure of the circulation. A qualitatively correct kinetic energy spectrum is produced when the resolution is high enough to include several linearly stable modes. A model with three zonal waves and the first three meridional modes has a reasonable energy spectrum and energy conversion cycle, while also satisfying heat and momentum budget requirements. This truncation reproduces the basic mechanisms and zonal circulation features that are obtained at higher resolution. The model performance improves gradually with higher resolution and is smoothly dependent on changes in external parameters.

1. Introduction

Low-order models are useful for studying fundamental dynamical and physical processes in the atmosphere because they distill these processes down to their simplest possible manifestation. An obvious question which arises about low-order models is whether they remain valid when more degrees of freedom are permitted. The topographically-induced, multiple equilibria of Charney and Straus (1980) were destabilized and, thus, were not realizable when an extra zonal wave was included (Reinhold and Pierrehumbert, 1982, henceforth referred to as RP). Instead, for a limited parameter range, RP found "weather regimes", i.e., quasi-stationary behavior of the long wave in opposite phases. The weather regimes, in turn, vanished as more waves were added by Cehelsky and Tung (1987, henceforth referred to as CT). They found that the model converged to a single long-wave regime as the resolution was increased.

In this paper we investigate the ability of low-order, two-layer models to reproduce the essential elements of the mid-latitude general circulation. We show that many fundamental processes and structures of the mid-latitude circulation are successfully reproduced if the model resolution exceeds a critical truncation level. Above this truncation level, model behavior does not qualitatively change with increasing resolution. The model is more responsive to changes in external parameters than to changes in resolution above this truncation level. If the resolution is below this level, the model is structurally incapable of reproducing several basic features of the circulation.

Tung and Rosenthal (1987) and CT have suggested that external momentum forcing is necessary to obtain realistic zonal winds in the lower layer of two-layer models. This forcing is intended to represent subtropical eddy momentum flux into mid-latitudes. Such forcing is not included in our model. Instead, qualitatively realistic surface winds are generated by internal momentum transports. A reasonable surface wind distribution was similarly obtained by Phillips (1956) in his original two-layer model. For a realistic surface wind distribution, a low-order model must have sufficient meridional resolution to allow eddy momentum flux convergence in the gravest meridional mode.

Many features of mid-latitude dynamics can be simulated in a two-layer, β-plane channel model with just three waves in both the zonal and meridional directions. A model with this truncation can be useful for investigations of extratropical dynamics and climate. It is very simple and inexpensive to integrate, and does not retain several undesirable features which are present in more severe truncations.

The criteria used for measuring the quality of the model are discussed in the following section. The model formulation is outlined in Section 3. Section 4 contains results of a linear stability analysis. Physical and geometrical constraints in the model are discussed in Section 5. Model behavior at different truncations is presented in Section 6, followed by a concluding discussion in Section 7.

2. Criteria used for model evaluation

The mean meridional circulation (MMC), time-mean temperature and zonal wind fields, and time-mean heat and momentum budgets all have large-scale meridional structures as shown by Newell et al. (1972) and Oort (1983). The dominance of large scales suggests that models with low meridional resolution may be successful in modeling the basic structures of the zonally averaged, mid-latitude circulation. Furthermore, relatively few *zonal* waves may be needed to model the large-scale balances, as in the two-level primitive-equation model of Held and Suarez (1978). The qualitative characteristics of the zonal-mean circulation were reproduced by that model using only zonal wavenumbers 3 and 6.

The following features are used as criteria for success in our model.

- Time-mean surface westerlies at appropriate latitudes and realistic strength and structure of upper-level winds;
- Realistic temperature gradients;
- A vertically averaged momentum balance between eddy momentum flux convergence and surface friction;
- A mean heat balance between diabatic heating, eddy heat flux convergence, and transport by mean meridional circulations;
- A realistically large amount of flow variability;
- A reasonable kinetic energy spectrum and energy conversion cycle.

In addition, a reliable low-order model should be smoothly sensitive to the model discretization, spectral truncation, and details of physical parameterizations. Certain singularities due to approximation cannot be avoided in two-layer models. For example, the critical shear for baroclinic instability is an artifact of the vertical discretization. Likewise, the weather regimes described by RP are an artifact of the truncation and parameter setting, as demonstrated by CT and O'Brien and Branscome (1988).

Because our emphasis is on the low-order statistics of the zonally-averaged circulation, external zonal asymmetries, such as topography, are excluded from our model. We also neglect the effects of moisture and latent heat release. A hydrological cycle is vital to any comprehensive general circulation model, as are many other physical processes which we omit. We will concentrate on some fundamental issues in low-order modeling and identify a dynamically accurate model which should produce credible results when moisture and bottom topography are included.

3. Model formulation

We use the same basic formulation as Yoden (1983), CT, and O'Brien and Branscome (1988). Let the subscripts u and l refer to the upper and lower layers, respectively. Let $\psi = (\psi_u + \psi_l)/2$ be the barotropic streamfunction, $\tau = (\psi_u - \psi_l)/2$ the baroclinic streamfunction, $\theta = (\theta_u + \theta_l)/2$ the mean potential temperature, and $\sigma = (\theta_u - \theta_l)$ the static stability, which is assumed constant. The governing equations are the barotropic and baroclinic vorticity equations and the thermodynamic equation:

$$\partial \nabla^2 \psi/\partial t = -J(\psi, \nabla^2 \psi) - J(\tau, \nabla^2 \tau) - \beta\, \partial\psi/\partial x - 0.5k\,\nabla^2(\psi - 2\tau) - \nu\,\nabla^{2p}\psi, \quad (1)$$

$$\partial \nabla^2 \tau / \partial t = -J(\psi, \nabla^2 \tau) - J(\tau, \nabla^2 \psi) - \beta \partial \tau / \partial x - fw/H + 0.5k\nabla^2(\psi - 2\tau) - \nu \nabla^{2p} \tau, \quad (2)$$

$$\partial \theta / \partial t = -J(\psi, \theta) - \sigma w/H + \eta(\theta^* - \theta). \quad (3)$$

Here f and β are the Coriolis parameter and its derivative at the center of the channel, respectively, k the Ekman damping coefficient at the surface, H the thickness of each layer, w the vertical velocity at the interface, η the Newtonian cooling coefficient, θ^* a prescribed potential temperature field in radiative equilibrium, ν a diffusion coefficient, p some positive integer and J the horizontal Jacobian. The system of equations is closed by the thermal wind relation

$$\nabla^2 \theta = A \nabla^2 \tau, \quad (4)$$

where A is a constant factor as in RP and CT.

Our model differs from CT's formulation in the parameterizations of frictional dissipation. Ekman friction in our model acts on surface wind, as determined by linear extrapolation (Phillips, 1956), rather than on lower layer wind. No interfacial friction is present, but horizontal diffusion of variable order acts on vorticity in each layer. Note that the sign of the diffusion terms in (1) and (2) would change if p is even.

We assume the channel is periodic in x over the scale $2\pi L/n$ with no flow through, or net drag on, the walls at $y = 0$ and $y = \pi L = 5000$ km. The parameter n is the fundamental zonal wavenumber and is related to planetary zonal wavenumber, m, by $m = na_0 \cos\phi_0/L$, where a_0 is the earth's radius and ϕ_0 is the central latitude of the channel. All dependent variables and the specified θ^* field are non-dimensionalized and expanded in the orthonormal eigenfunctions, $F_i(x, y)$, of the Laplace operator. The three sets of basis functions, F_i, which represent the horizontal structure are given by:

$$FS_{(i,j)} = 2\sin(jy)\sin(inx),$$

$$FC_{(i,j)} = 2\sin(jy)\cos(inx),$$

$$FM_{(j)} = \sqrt{2}\cos(jy). \quad (5)$$

The fundamental zonal wavenumber, n, may be chosen freely. A (M, N)-resolution model retains the basic functions, F_i, with (x, y) wavenumbers (i, j) up to and including (M, N).

The set of spectrally decomposed equations is similar to the sets in CT and O'Brien and Branscome (1988) and is not repeated here. After eliminating w between (2) and (3) and using (4), the spectral model consists of $2N(2M+1)$ ordinary differential equations for the amplitude coefficients of the $N(2M+1)$ eigenfunctions of the streamfunction, ψ, and potential temperature, θ. The only θ^* component taken different from zero corresponds to $FM_{(1)}$, so that the radiative forcing is given by the dimensionless parameter $\theta^*_{M(1)}$. The external parameters are assigned the values:

$$\eta = (14.0 \text{ days})^{-1}, \quad k = (5.6 \text{ days})^{-1}, \quad \theta^*_{M(1)} = 0.06,$$
$$\beta = 1.44 \times 10^{-11} \text{ m}^{-1}\text{ s}^{-1}, \quad \sigma = 34\,^\circ\text{C}, \quad n = 1.3. \quad (6)$$

These values correspond to a radiative equilibrium temperature difference of 50°C across a channel centered on 51° latitude, a Brunt-Väisälä frequency of 10^{-4} s^{-2}, and a fundamental zonal wavenumber of $m = 3$ or a wavelength of about 8000 km. These values will be referred to as the "standard" set of parameters and are used in all model runs except where specifically stated.

We included horizontal diffusion to compensate for short, unresolved scales which, if they were included, would damp larger, resolved scales and reduce total eddy kinetic energy (EKE). Without any diffusion, EKE remains unrealistically large. After some experimentation, we chose a scale-uniform ∇^2 damping (i.e., $p = 1$) rather than a higher power, scale-selective diffusion because the problem was with *total* EKE and not with the spectral distribution of energy. This diffusion does not operate on the zonal mean flow, since it would weaken the lower-layer westerlies to the extent that surface winds would be easterly everywhere. The inclusion of internal vorticity damping did not affect the primary balances and mean circulations. Our standard parameter set uses a ν which corresponds to an e-folding period of 56 days, or ten times longer than surface friction.

The thermal forcing, $\theta^*_{M(1)}$, was varied between zero and 0.2 by Charney and Straus (1980) and Yoden (1983), while RP and CT both used the fixed value of $\theta^*_{M(1)} = 0.1$. We found that the value of 0.1 led to unrealistically large energy conversions and EKE. Reducing the radiative equilibrium temperature gradient had a salubrious effect on EKE and energy conversions, which were much more sensitive than zonal available potential energy (zonal APE) to the strength of the radiative forcing. Furthermore, Stone (1972) gives an estimate of -0.95°C per 100 km for the earth's meridional temperature gradient in radiative-convective equilibrium. This gradient translates to a temperature difference of about 48°C across our 5000 km channel, which compares well with our value of $\theta^*_{M(1)}$.

The Lorenz N-cycle scheme with $N = 4$ (Lorenz, 1971) was used for the time integration. Unless indicated otherwise, the model was integrated for 600 days with the last 500 days used for statistical purposes. The model was initialized with a symmetric equilibrium flow in the $FM_{(1)}$ mode, along with small perturbations in all other modes. The symmetric equilibrium state simply corresponds to zonal flow in thermal wind balance with the θ^* field.

4. Linear stability analysis

Prior to running the time-dependent model, we investigated the linear stability properties of the symmetric or radiative equilibrium flow. This stability analysis is helpful in understanding the behavior of the time-dependent flow and provides an approximate upper bound on linear instability in the full model. We considered the stability of the radiative equilibrium state with respect to perturbations in each (i, j) mode separately. Charney and Straus (1980) used the same procedure for instability calculations in a low-order model. This procedure differs from the approach of Pedlosky (1964), who solved for the meridional structure of a perturbation as a function of zonal wavenumber and obtained neutral curves which were functions of zonal wavenumber alone. In our analysis, different meridional modes are selected one at a time and neutral stability curves are obtained as functions of meridional mode as well as zonal wavenumber.

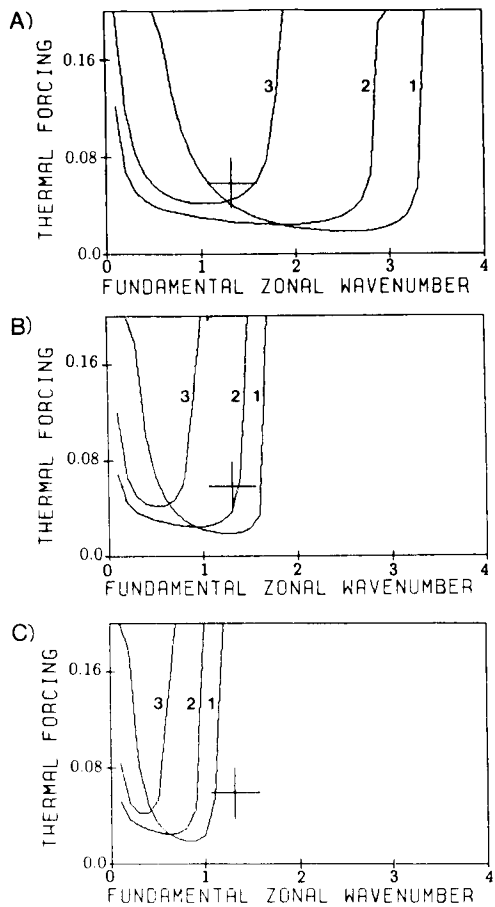

Fig. 1. Neutral curves for linear baroclinic instability of the radiative equilibrium state. The ordinate is thermal forcing $\theta^*_{M(1)}$ and the abscissa is the fundamental zonal wavenumber n. The + represents the $(n, \theta^*_{M(1)})$ setting at which the models were run. (a) Neutral curves for the $(1x, 1y)$, $(1x, 2y)$, and $(1x, 3y)$ modes. Meridional mode number is shown on each curve. Neutral curves for meridional mode of four or higher do not reach down into area of plot. (b) As in (a) but for the $(2x, 1y)$, $(2x, 2y)$, and $(2x, 3y)$ modes. (c) As in (a) but for the $(3x, 1y)$, $(3x, 2y)$, and $(3x, 3y)$ modes.

Fig. 1 shows the neutral curves for the nine largest-scale modes as functions of fundamental zonal wavenumber n and external forcing $\theta^*_{M(1)}$, with all other parameters as in the standard set. The plus sign in Fig. 1 marks the setting at which the full model is run. Five modes, $(1x, 1y)$, $(1x, 2y)$, $(1x, 3y)$, $(2x, 1y)$, and $(2x, 2y)$, are linearly unstable for this parameter set. All unstable waves, plus some stable ones, must be included in the time-dependent model to provide a proper pathway for energy and enstrophy transfer and prevent the build-up of energy in the shortest resolved scale in a "spurious chaos" (Curry et al., 1984). Based on this criterion, the model should have at least a (2, 3) resolution, i.e., $M = 2$ and $N = 3$.

These same five modes remain the only unstable waves for a wide range of the parameters. Only the $(1x, 3y)$ wave is linearly stabilized for the parameter set in RP and CT (which differs from our standard set by changing surface friction, interface friction, and radiative time scales to approximately 1 day, 10 days, and 2.5 days, respectively). The neutral curve for the most unstable wave (i.e., the $(2x, 1y)$ mode) is not very sensitive to an order of magnitude increase or decrease in the surface friction parameter.

In fact, the only parameter which has a large impact on the stability of the waves is the static stability, σ. Ideally, a model of the general circulation should determine the value of σ internally, as a function of space and time. Unfortunately, σ is an externally prescribed constant in our model and is set to a typical atmospheric value.

The radiative equilibrium state in our experiments is unstable only to the five modes mentioned above. However, some of these modes may be excluded by the truncation. The model behaves quite differently in truncations which include only unstable modes from truncations which also include several stable modes. The model is dominated by linear instability mechanisms in the former case and by nonlinear wave-wave interactions in the latter.

5. Physical and geometrical constraints of different model resolutions

5.1. Properties of the interaction coefficients

Nonlinear processes in the model are effected through interaction coefficients which are described in detail in the appendix. It is evident from (A3) that interactions between two different zonal wavenumbers cannot occur in a model which retains only odd meridional modes. For some experiments it was instructive to eliminate wave-wave interactions by retaining only odd meridional modes. On the other hand, (A4) and (A5) show that only one zonal wave at a time is involved in wave-mean flow interactions, which can occur when only odd meridional modes are retained, but not when only even modes are retained.

It is also evident from (A1) and (A3) that the shortest wave in a (2, 2) model cannot participate in wave-wave interactions. Consequently, an unrealistic amount of energy is present at this scale in a (2, 2) model using our standard parameter set (O'Brien and Branscome, 1988). The unstable $(2x, 2y)$ wave becomes the dominant mode in a (2, 2) model since it gains energy from the mean flow, but cannot lose energy to other waves. The shortest scale in a model with higher resolution is never likely to dominate because it would be linearly stable for our parameter setting. However, the shortest scale in truncations higher than a (2, 2) model can be excited by wave-wave interactions.

5.2. Heat and momentum budgets

We now consider the constraints placed on the heat and momentum balances by the choice of spectral truncation. The time-mean, zonally averaged thermodynamic equations leads to a balance among the following terms:

$$-[\overline{v'\theta'}]_y - \sigma_0[\overline{w}] + \eta[\overline{\theta^*} - \overline{\theta}] = 0. \tag{7}$$

Here $(\cdot)_y$ represents the partial derivative with respect to y, $[\cdot]$ the zonal average, $(\cdot)'$ a deviation from the zonal average and the overbar a time mean. The terms in (7) represent eddy heat flux convergence, transport by mean meridional circulations, and diabatic forcing, respectively. We have assumed in (7) that the averaging period is sufficiently long to ensure to a negligible time derivative. A minimal model of (1, 1) truncation is sufficient to resolve a heat balance between diabatic heating and eddy flux convergence of a single baroclinic mode. The mean meridional circulation term, $\sigma_0[\overline{w}]$, is negligible unless the meridional resolution retains at least the first and third meridional modes, as we shall see presently.

The time-mean, zonally and vertically averaged momentum balance can be found by integrating the barotropic vorticity equation (1) with respect to y, which gives

$$[\overline{\psi_x \psi_y}]_y + [\overline{\theta_x \theta_y}]_y + 0.5k[\overline{\psi} - 2\overline{\theta}]_y = 0. \tag{8}$$

The first two terms in (8) together represent the divergence of vertically averaged eddy momentum flux. This momentum transport maintains the zonal winds against surface friction, which is represented by the third term in (8).

The surface friction in (8) has the meridional dependence $\sin(jy)$, for each mode j. Integrating (8) across the channel demonstrates that the meridional integral of mean surface wind must be zero. This requirement is automatically satisfied for even meridional modes, but not for odd modes, since $\int_0^\pi \sin(jy)\,\mathrm{d}y = 0$ only if j is even. The structure of modes in a $(M, 1)$ model prohibits eddy momentum flux so that the mean surface wind must be zero. Eddy momentum flux divergence can occur in a $(M, 2)$ model, but has a projection onto the $\sin 2y$ structure only. Thus, the mean surface wind has no $\sin y$ component and is antisymmetric about the center of the channel. The constraint on mean surface winds is trivially satisfied in $(M, 1)$ and $(M, 2)$ models.

Once another odd mode is included, eddy momentum flux convergence into the $\sin y$ mode can occur and maintain the surface wind in this mode against dissipation. Net westerlies in one odd mode can be balanced by net easterlies in the other and the constraint on the total surface wind can be satisfied. Thus, a positive first mode ($\sin y$) component can combine with a negative third mode ($\sin 3y$) component to give a band of surface westerlies in the center of the channel, with narrower bands of easterlies to the north and south. Components of any number of odd modes can balance similarly.

These geometric considerations show that at least two odd meridional modes are needed to obtain mean surface winds which are symmetric about the center of the channel. When these modes are included, the symmetric components of momentum flux divergence and mean zonal wind consistently determine the structure of the flow, as shown in Section 6. Furthermore, truncations with more than one odd meridional mode allow upper-layer westerly winds to be concentrated into jets.

The momentum balances for the lower and upper layers, respectively, are

$$[\overline{\psi_{l_x}\psi_{l_y}}]_y - \int^y [\overline{w}]\,\mathrm{d}y' + k[\overline{\psi - 2\theta}]_y = 0, \tag{9}$$

$$[\overline{\psi_{u_x}\psi_{u_y}}]_y + \int^y [\overline{w}]\,\mathrm{d}y' = 0. \tag{10}$$

Note that the MMC terms in (9) and (10) are indefinite y-integrals (not integrals across the entire channel) and have opposite effects in the upper and lower layers. No eddy momentum flux is allowed in $(M, 1)$ models and, consequently, no forcing of the MMC occurs in (10). Eddy momentum flux can occur in $(M, 2)$ models and force a MMC with a $\sin 2y$ meridional structure. However, the flux divergence is antisymmetric about the center of the channel and should be small when averaged over a long period of time. Momentum flux convergence in $(M, 3)$ models is permitted in all three meridional modes and a three-cell MMC is possible. If eddy momentum flux in the lower layer is negligible, the MMC will induce surface winds by vortex stretching in the lower layer, as shown in (9).

It is geometrically possible for the MMC and mean surface winds in a $(M, 3)$ model to be reversed from the observed sense of circulation. However, this configuration is unlikely to occur, for reasons given by Held (1975). He showed that growing waves in two-layer models will cause a net flux of westerly momentum into regions with strong vertical shear, or more precisely, where the zonal-mean vorticity gradient in the lower layer is negative. The vertical shear in our model is always strongest in the middle of the channel, coincident with the strongest gradient in radiative equilibrium temperature. Therefore, momentum flux convergence will maintain surface westerlies in the middle of the channel rather than near the walls.

6. Model results for various truncations

6.1. *Time-mean temperature and wind fields*

Higher meridional and zonal resolution may allow more complicated structures to appear in the zonal circulation. To investigate this possibility, the full time-dependent model was run at various truncations. Unless otherwise stated, our standard set of external parameters was used, along with the 56-day ∇^2 damping discussed in Section 3.

Fig. 2 shows time-mean zonal wind distributions at different levels for (2, 2), (3, 3), (5, 5), and (3, 9) models. The surface wind distribution, $[\overline{\psi - 2\theta}]_y$, is the leftmost curve for each of the truncations shown in Fig. 2. The middle curves in Fig. 2 are the mid-level or barotropic wind, $[\overline{\psi}]_y$, and the rightmost curves are the upper level wind, $[\overline{\psi + \theta}]_y$.

The most dramatic differences between various truncations are apparent in the surface winds. Surface winds in the (2, 2) model (Fig. 2a) are negligibly weak everywhere. On the other hand,

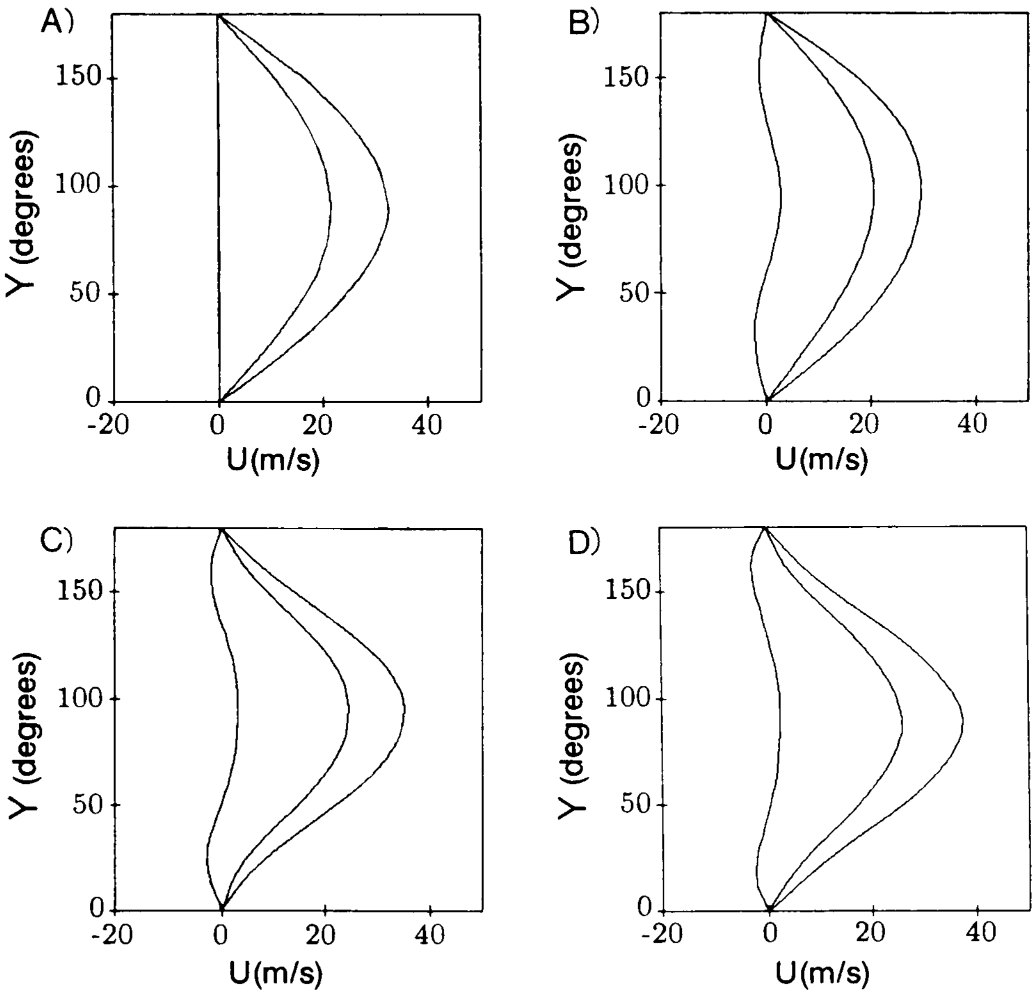

Fig. 2. Time-mean zonal wind distributions for: (a) the (2,2) model; (b) (3,3) model; (c) (5,5) model; and (d) (3,9) model. In all cases, the leftmost curve is surface wind, the middle curve is mid-level wind, and the rightmost curve is upper-level wind. Meridional distance is scaled and appears in degrees (with 180 corresponding to the northern wall).

the (3,3) model (Fig. 2b) has surface westerlies in the middle of the channel with narrower bands of easterlies near the walls. The same structure is apparent in the (5,5) and (3,9) models (Figs. 2c, d). The circulations in (4,4) and (6,6) models (not shown) closely resemble the (3,3) and (5,5) cases, respectively, while (3,5) and (3,7) (not shown) models are very similar to the (3,9) case. The major qualitative change in the surface wind occurs when the meridional resolution is increased from two modes to three. Surface zonal wind strengths at the center of the channel are given in Table 1 for different truncations.

Mid- and upper-level winds are comparable in all truncations. However, the (3,9) and (5,5) models (Figs. 2c, d) and other truncations with high meridional resolution permit some tightening of the zonal flow into a jet. The time-mean zonal flow is essentially symmetric about the midpoint of the channel, although some small contributions from asymmetric meridional modes can be seen. The departure from symmetry about the center of the channel appears to be random, since integrations with the (5, 5) model using slightly different initial conditions led to varying, but generally small, contributions from asymmetric modes.

The major qualitative changes in zonal-mean circulation evident in Fig. 2 are primarily dependent on meridional resolution and are unaffected by the presence or absence of wave-wave interactions. Similar changes with increasing meridional resolution occur in the absence of wave-wave interactions, i.e., when only odd meridional modes or only one zonal wavenumber are retained. The addition of more zonal scales or meridional modes higher than three contribute minor corrections to the basic structure established by the first and third meridional modes.

The main factor determining upper-level wind strength is the mean meridional temperature gradient. Because the heat balance is dominated by unstable modes, which are present even in the (2, 2) model, the mean temperature gradient is very similar in all truncations. It suffices to show, in Fig. 3, the time-mean temperature for the (3, 3) case only. The corresponding radiative equilibrium temperature is also shown. The mean temperature gradient is nearly independent of y over a large part of the channel and, at the center, is about 60% larger than the minimum gradient required for instability of the most unstable mode (i.e., the $(2x, 1y)$ mode). The radiative equilibrium gradient at the midpoint is about 3.5 times larger than the minimum gradient for instability.

The standard radiative forcing is sufficiently strong to cause baroclinic instability and the equilibrated temperature gradient in the model is supercritical by the measure of linear instability. We did not examine the effectiveness of baroclinic adjustment by the waves over a wide parameter range. Using a similar model, Ebisuzaki (1988) has shown that the degree of supercriticality is a function of several parameters, including radiative forcing, dissipation, and channel width. We found that eddy energy in our model was much more sensitive than zonal available potential energy to changes in the radiative equilibrium gradient. This behavior suggests that baroclinic waves and their heat transports amplify in response to increases in supercriticality and provide a strong negative feedback on the mean temperature gradient. A similar response was found by Held (1978) in the low-order model of Held and Suarez (1978).

The supercritical shear becomes slightly enhanced as more waves are included in the model (Table 1). The increase in supercriticality is due to enhanced wave-wave interactions, which effectively damp very unstable waves by allowing energy transfer to stable (or less unstable) modes. The impact of nonlinear transfer on the mean shear equilibration is also reflected in a higher standard deviation (4–5°C) of the cross-channel temperature difference in the (3, 3), (5, 5), and (3, 9) models than the 1°C standard deviation found in the (2, 2) model, which has relatively few wave-wave interactions.

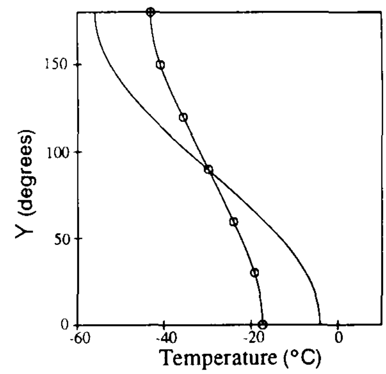

Fig. 3. Time- and zonal-mean temperature (curve with circles) and radiative equilibrium temperature (no symbols) for the (3, 3) model.

Table 1. *Time-mean values of surface wind at the center of the channel, $\theta_{M(l)}$, and cross-channel temperature difference for different truncations*

Resolution	Mean surface U (m s^{-1})	Mean $\theta_{M(1)}$	Mean ΔT (°C)
(2, 2)	0.0	0.0359	26.7
(3, 3)	2.7	0.0333	25.6
(4, 4)	3.1	0.0341	25.9
(5, 5)	2.4	0.0365	26.8
(6, 6)	3.4	0.0373	27.2
(3, 5)	2.7	0.0361	26.6
(3, 7)	3.0	0.0372	27.5
(3, 9)	2.4	0.0375	27.5

Nonlinear damping of unstable modes allows the flow to equilibrate at supercritical levels (Vallis, 1988) or, more precisely, inhibits the effectiveness of the baroclinic adjustment process proposed by Stone (1978). Alternatively, Reinhold (1988) has suggested that constraints on the structure of long baroclinic waves lead to large amplitudes for the long waves and supercritical equilibration of the mean flow with respect to shorter, more unstable wavelengths. Vallis (1988) has shown that nonlinear interactions among just three modes are sufficient to cause supercritical equilibration. When we ran our model with either the $(1x, 1y)$ or $(2x, 1y)$ mode only, the mean temperature gradient equilibrated at the critical shear for that particular mode. However, the mean shear in the (2, 2) model was close to the critical shear of the $(1x, 1y)$ mode, but substantially supercritical with respect to the critical shear of the $(2x, 1y)$ mode. A similar behavior of mean flow equilibration was found by CT.

6.2. *Time-mean heat balances*

The time-mean, zonally averaged heat balance (7) is shown in Figs. 4–6 for various truncations. Diabatic heating is balanced by only eddy flux divergence in a (2, 2) model. The MMC does not contribute to the heat balance of a (2, 2) model for the reasons stated in Subsection 5.2. However, the MMC is present in the (3, 3) model (Fig. 5) and has an obvious $\cos 3y$ structure.

Modifications to this structure are apparent in the (5, 5) model (Fig. 6), as a $\cos 5y$ correction is added to the basic $\cos 3y$ pattern. However, this correction does not change the fundamental 3-cell MMC and surface wind structure. Heat balances in a (6, 6) model and models with high meridional resolution are very similar to the balance in the (5, 5) model. Corrections due to even y-modes are negligible, while corrections due to odd modes are successively smaller and all have the same (positive) sign as $w_{M(3)}$.

6.3. *Time-mean momentum balances*

The vertically-averaged momentum balance (8) is shown in Figs. 7–9 for various truncations. The most obvious changes occur as resolution is increased from (2, 2) (Fig. 7) to (3, 3) (Fig. 8). Note that the terms in the (2, 2) model are about two orders of magnitude smaller than in the higher order models. All terms in the (2, 2) case must

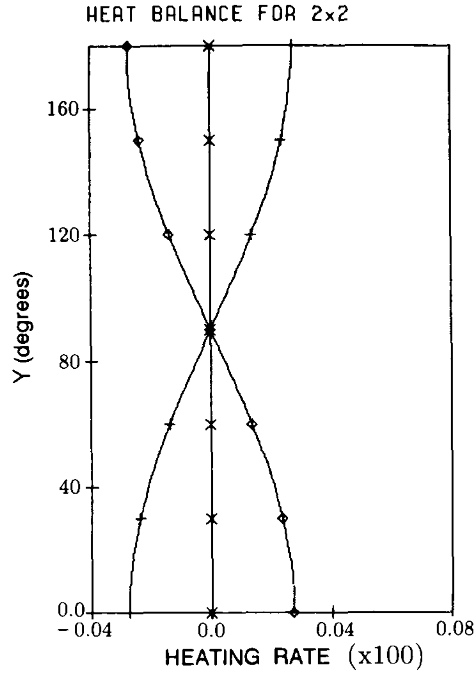

Fig. 4. Meridional structure of the time-mean, zonally averaged heat balance for the (2, 2) model. Diabatic heating is labelled with diamonds, eddy heat flux convergence with plus signs and MMC heating with X. The abscissa is nondimensional, but the maximum value of diabatic heating is about 0.8 °C per day.

have a $\sin 2y$ structure and so the balance is asymmetric about the center of the channel. The odd meridional modes in the (3, 3) and (5, 5) (Fig. 9) models permit surface wind components and momentum flux convergences in each mode, as discussed in Subsection 5.2. Eddy momentum flux convergence maintains the surface westerlies against dissipation in the middle of the channel, and flux divergence maintains easterlies near the channel walls. Once this symmetric configuration is permitted, it dominates the asymmetry of even meridional modes. The balance does not change qualitatively as more zonal waves or meridional modes are added; the three-lobe structure remains, even in a (3, 11) model (not shown).

The dominant balance in the lower-layer momentum budget (9) is between MMC transports and surface friction, which is also the principal balance in the lower troposphere in midlatitudes (Newell et al., 1972). The MMC term determines the direction of the surface wind in

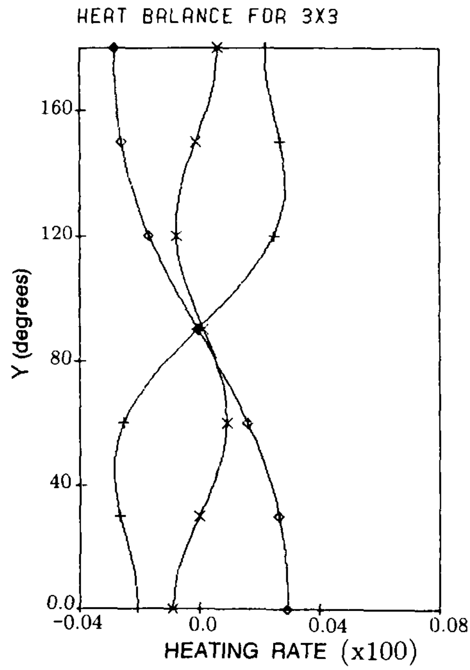

Fig. 5. As in Fig. 4 but for the (3, 3) model.

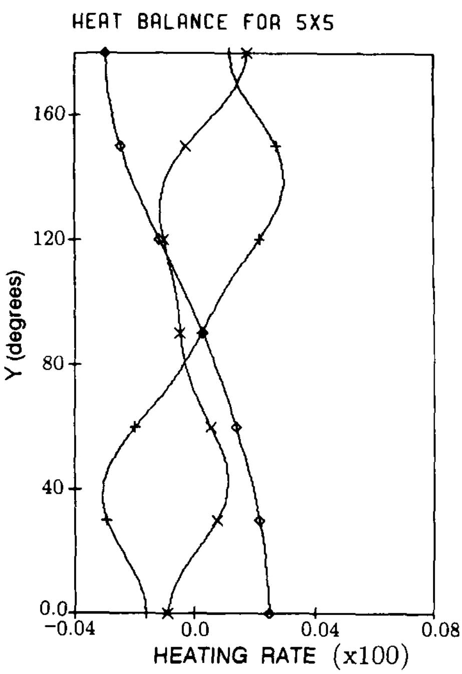

Fig. 6. As in Fig. 4 but for the (5, 5) model.

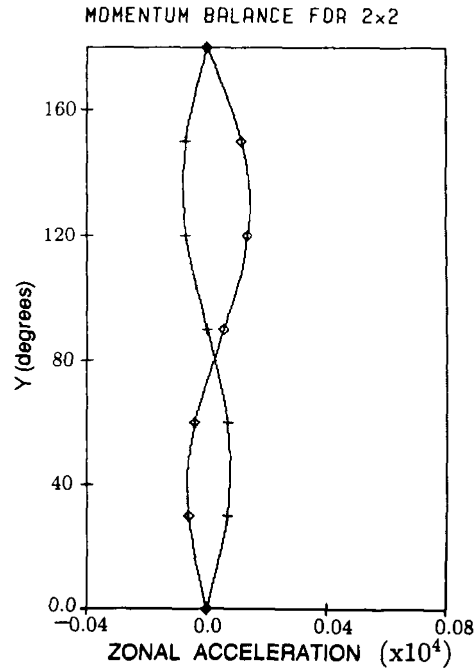

Fig. 7. Meridional structure of time-mean, vertically and zonally averaged momentum balance for the (2, 2) model. Surface friction is labelled with diamonds and eddy momentum flux convergence with plus signs. Magnitudes are non-dimensional, but 10^{-4} corresponds to an acceleration of about 0.15 m s^{-1} day^{-1}.

every truncation, as described in Subsection 5.2. The eddy momentum flux divergence in the lower layer has the opposite sign and is smaller than the divergence in the upper layer, which determines the sign of the vertically averaged flux divergence and direction of the MMC.

We have shown that the meridional structure of the mean circulation and heat and momentum budgets depend on meridional resolution. If three or more meridional modes are retained, this structure is independent of the number of zonal waves and the presence of wave-wave interactions. This conclusion has been verified by running the model with different numbers of zonal waves and by including odd meridional modes only.

6.4. *Spectral energetics*

The spectral energy distribution is highly dependent on whether or not wave-wave interactions are permitted. These interactions provide

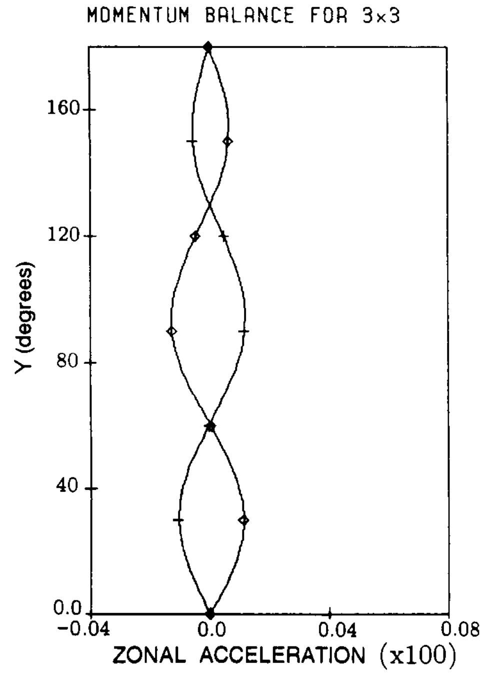

Fig. 8. As in Fig. 7 but for the (3, 3) model.

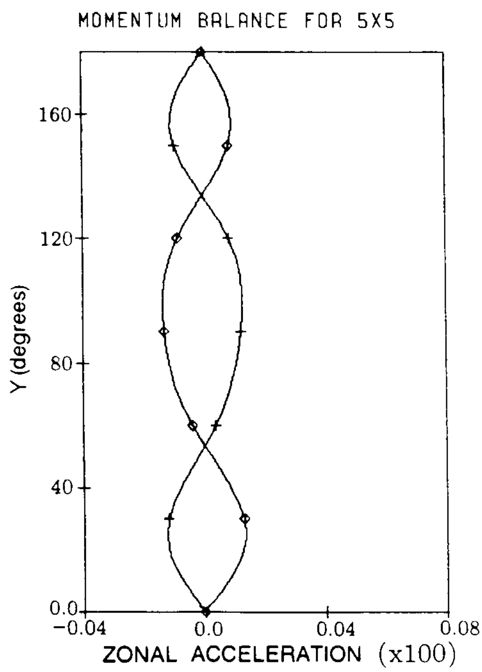

Fig. 9. As in Fig. 7 but for the (5, 5) model.

an energy transfer mechanism (described by Rhines, 1977; Salmon, 1980; and others) which smooths and reddens the energy spectrum. Nonlinear interactions distort the linear stability properties of long, unstable waves and are enhanced when short, linearly stable waves are present. Wave-wave interactions provide the only energy source for short zonal waves. When these interactions are excluded, only zonal wavenumbers one and two become excited, even if higher wavenumbers are permitted by the truncation. All modes with zonal wavenumber three or higher are linearly stable in a model using our standard parameter set and cannot grow in the absence of wave-wave interactions. A (3, 3) or higher order model with no wave-wave interactions has a sharp decrease in energy between zonal wavenumbers two and three at all meridional scales.

On the other hand, long zonal waves with very short meridional scales are excited in the absence of wave-wave interactions, even though these modes are linearly stable. In this case, wave-mean flow interactions transfer some energy to small meridional scales and maintain a meridional energy spectrum which facilitates a consolidation of the three-cell MMC. A smooth energy spectrum, with energy at all scales, is established in (1, 9) and (2, 9) models with and without wave-wave interactions. In fact, more energy is present at short scales in a (2, 9) model if wave-wave interactions are excluded.

The kinetic energy spectra of (2, 2), (3, 3) and (5, 5) models are shown in Fig. 10. As mentioned

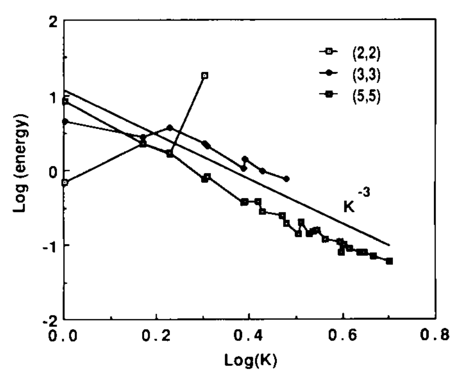

Fig. 10. Kinetic energy spectrum as a function of total wavenumber, K, for (2, 2), (3, 3) and (5, 5) models. A K^{-3} profile is also shown.

in Subsection 5.1, a spurious energy build-up occurs at the shortest scale of the $(2x, 2y)$ model, which has no linearly stable modes. Kinetic energy in a (2, 3) model (not shown) is distributed fairly evenly among the resolved scales. Thus, a (2, 3) truncation, which retains only one unstable mode, allows only marginal operation of nonlinear energy transfer. The maximum energy at higher truncation resides in the largest scale, the $(1x, 1y)$ mode, which corresponds to planetary wavenumber 3. The spectra in the (3, 3) and (5, 5) models have approximate k^{-3} distributions at the small scales. As the resolution is increased, total eddy kinetic energy gradually decreases because of the dissipative effects of additional short waves.

This spectrum would probably continue to "converge" as the resolution is increased beyond the (6, 6) case, which is our highest resolution. Since convergence is slow, it would be impractical to seek the converged state, using the interaction coefficient method. The most important result presented here is the critical change in the nature of the spectrum once linearly stable waves are included. When this condition is met, the energy spectra in the model shows a decay of energy with scale that is consistent with much higher resolution models (e.g., Salmon, 1980; Vallis, 1983).

We also integrated a (5, 5) model with the fundamental wavenumber n reduced from 1.3 to 0.9, i.e., the planetary wavenumber m was reduced from about 3 to 2. The linear stability curves in Fig. 1 indicate that the $(1x, 1y)$ wave is stable for this value of n. However, the $(3x, 1y)$ and $(3x, 2y)$ waves become unstable, while shorter modes remain stable. Therefore, a minimum resolution of (4, 3) is necessary to include all unstable modes in this case. The kinetic energy spectrum in a (5, 5) model with $n = 0.9$ decays smoothly at short scales, but peaks at the $(2x, 1y)$ mode instead of the $(1x, 1y)$ mode. Nonlinear processes still put a significant amount of energy into the stable $(1x, 1y)$ wave so that this scale has only slightly less energy than the $(3x, 1y)$ wave, which is the most unstable mode.

These results are consistent with integrations using $n = 1.3$, which resolves planetary wavenumbers $m = 3, 6, 9, \ldots$. The maximum energy in the $n = 1.3$ case resides in $m = 3$, which is the longest zonal wave in the model. Planetary wavenumbers 2, 4, 6, etc. are resolved when $n = 0.9$, and the peak in energy occurs at $m = 4$. If the fundamental planetary wavenumber were reduced to $m = 1$ (equivalently, $n = 0.4$), it is likely that either planetary wavenumber 3 or 4 would be the most energetic as found by Salmon (1980). The disadvantage of reducing n is that more waves must be included by the truncation in order to include all unstable modes.

6.5. *Channel energetics*

The energy budget does not vary significantly with truncation, as seen from Lorenz energy diagrams for the (2, 2), (3, 3), and (5, 5) models (Fig. 11). Zonal KE and APE, as well as the principal conversions, differ relatively little between various truncations. Comparisons with similar diagrams for the atmosphere (Oort, 1964) or for a composite of quasi-geostrophic models (Wiin-Nielsen, 1968) suggest that the conversions and energies in Fig. 11 are qualitatively correct. One exception is that no generation of eddy APE (EAPE) is permitted in the model. The generation of EAPE in the atmosphere can occur through latent heat release and continent-ocean contrasts, which are not included in the present model.

The standard parameter values were chosen as representative of atmospheric values, and they gave reasonable results for energetics and mean circulations. We have run the model with various parameter settings, varying the coefficient ν of the ∇^2 damping, surface friction time k^{-1}, Newtonian cooling time η^{-1}, and thermal forcing $\theta^*_{M(1)}$. We found a smooth dependence on these parameters as they were varied by a factor of two or more from their standard values. The structure of the zonal circulation and shape of the energy spectrum were not affected by these parameter changes. Only the strengths of energy densities and conversions were affected, primarily when $\theta^*_{M(1)}$ was changed.

Increasing ν in the ∇^2 damping had the specific effect of reducing EKE and did not significantly alter any other quantity. Even though it has a long time scale (56 days in the standard set), the ability of the ∇^2 damping to remove EKE is comparable to that of surface friction since it operates on the much stronger upper (and lower) layer winds. Fig. 12 shows Lorenz diagrams for (3, 3) runs with: (a) ν set to zero (all other

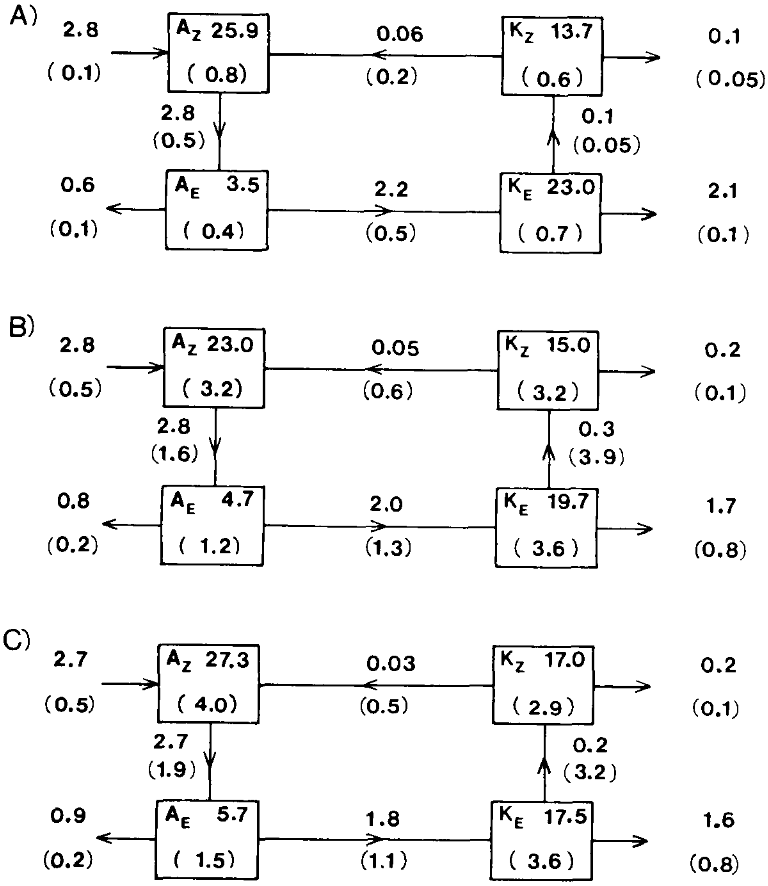

Fig. 11. Mean energy densities and conversions for: (a) the (2, 2) model; (b) (3, 3) model; and (c) (5, 5) model. Standard deviations of each quantity are in brackets. Zonal available potential energy is represented by A_Z; eddy APE by A_E; zonal kinetic energy by K_Z; and eddy kinetic energy by K_E. Generation, dissipation, and conversion terms are in the sense of the arrows. Energy densities are in 10^5 J m^{-2}, and conversions are in W m^{-2}.

parameters as in the standard set); and (b) $\nu = 0$ and $\theta^*_{M(1)}$ set to 0.1 (all others as in the standard set). The main differences between the results in Fig. 12 and Fig. 11b are found in EKE and, to a lesser extent, in EAPE.

7. Discussion

We have examined the impact of spectral truncation on the eddy dynamics and mean circulation of low-order, two-layer models. A single wavenumber in the zonal and meridional directions is sufficient to permit a zonally-averaged heat balance between diabatic forcing and eddy heat flux convergence. Due to momentum budget constraints, the MMC cells and time-mean surface winds may only exist when at least the first and third meridional modes are included. Model geometry and the structure of the radiative forcing dictate that terms in the heat budget are preferentially asymmetric about the center of the channel, while terms in the momentum budget are preferentially symmetric. Therefore, when three or more meridional modes are included, the momentum budget is dominated by the odd sine modes, especially modes one and three. Then

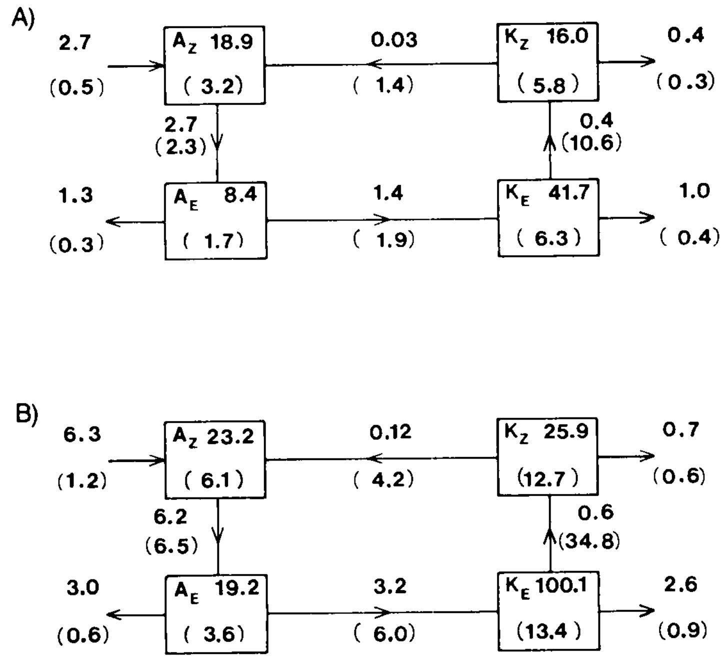

Fig. 12. Energy diagram for the (3, 3) model as in Fig. 11, but for (a) no ∇^2 damping, and (b) for no ∇^2 damping and $\theta^*_{M(1)}$ increased to 0.1.

momentum flux convergence maintains a band of surface westerlies at the center of the channel, and flux divergence maintains corresponding bands of surface easterlies near the walls.

Experiments with different truncations confirm that at least the first two odd meridional modes are needed for realistic circulations and balances. They also show that the inclusion of more modes does not qualitatively change model behavior. The three-cell MMC and three meridional bands of surface winds are persistent features, even when more complicated structure is permitted by the truncation. Higher modes provide corrections to "sharpen" the fundamental three-cell structure.

Only one *zonal* wavenumber is required for realistic heat and momentum balances. At least two waves are required for wave-wave interactions to occur, but at least three are required to include several linearly stable waves which can only be excited by these interactions. When several stable modes are included in the model, nonlinear interactions operate to produce a smooth energy spectrum with maximum energy in the longest scale and a decay of energy with total wavenumber. Energy transfers via these interactions can account for the supercritical equilibration of the mean shear with respect to the linearly most unstable wave, as demonstrated by Vallis (1988).

Increasing the resolution from the (3, 3) case has the effect of slowly modifying these results, reddening the spectrum further and reducing EKE. However, the energetics are more responsive to changes in certain external parameters. Some parameters are rather empirical, e.g., k, η, and the strength and order of horizontal diffusion. Suitable values for these parameters are not known precisely, so they may be "tuned" within reasonable ranges to give the most realistic behavior. We found that the model behavior always changed smoothly and in an intuitively predictable sense as external parameters were varied individually within moderate ranges. Most parameters in our model were set, a priori, to realistic values, although the thermal forcing and diffusion were moderately adjusted to improve model energetics.

The models did not reproduce perfectly all the mid-latitude circulation features listed in Section 2. However, our results suggest that a horizontal resolution of three modes in the zonal and meridional direction is sufficient to capture several essential features of the extratropical circulation and remove certain distortions caused by more severe horizontal truncation. Although these low-order models are limited by the channel geometry, constant static ability, lack of vertical resolution and many other approximations, their simplicity permits new insights into the dynamical processes of the atmosphere.

8. Acknowledgments

The first author is grateful for the support of a University of Miami fellowship during the early work on this paper. Both authors acknowledge the support of the Global Scale Atmospheric Processes Research Program of NASA Headquarters under Grant NAG8-656, administered by NASA Marshall Space Flight Center. We also wish to thank Prof. Peter Stone of M.I.T. for useful discussions and Prof. K-K. Tung for helpful comments.

9. Appendix

Given the different basis functions FS, FC, and FM, the nonlinear interaction coefficients may be defined as

$$c_{X(i,j)\,Y(p,q)\,Z(r,s)} = c'_{X(i,j)\,Y(p,q)\,Z(r,s)} - c'_{X(i,j)\,Z(r,s)\,Y(p,q)}, \tag{A1}$$

where X, Y, and Z each represent either an S, C, or M basis function,

$$c'_{X(i,j)\,Y(p,q)\,Z(r,s)} = \left\langle FX_{(i,j)}, \frac{\partial FY_{(p,q)}}{\partial x}\frac{\partial FZ_{(r,s)}}{\partial y}\right\rangle \tag{A2}$$

and $\langle F, G\rangle$ is the horizontal average of FG over the channel.

These coefficients represent the projection of the interaction between the (p,q) and (r,s) waves onto the (i,j) wave. If i, p, or r is zero, the mode corresponds to a zonal flow. For given wavenumbers i, j, p, q, r, and s, there are 3^3 or 27 possible c'_{XYZ}'s as X, Y, and Z represent different permutations of S, C, and M. However, only eight of these coefficients may be non-zero; four represent wave-wave interactions and four represent wave-mean flow interactions. The wave-wave coefficients are:

$$c'_{X(i,j)\,Y(p,q)\,Z(r,s)} = 0.5nps(\delta_{j=q+s} + \delta_{q=s+j} - \delta_{s=j+q})\Delta(i,p,r), \tag{A3}$$

where $\delta_g = 1$, if statement g is true, and is zero otherwise. The function $\Delta(i,p,r)$ is given by

$$\Delta(i,p,r) = \delta_{i=p+r} - \delta_{p=r+i} + \delta_{r=i+p}$$

when $(X,Y,Z) = (S,S,S)$; by

$$\Delta(i,p,r) = -\delta_{i=p+r} - \delta_{p=r+i} + \delta_{r=i+p}$$

when $(X,Y,Z) = (S,C,C)$; by

$$\Delta(i,p,r) = \delta_{i=p+r} + \delta_{p=r+i} + \delta_{r=i+p},$$

when $(X,Y,Z) = (C,S,C)$; and by

$$\Delta(i,p,r) = \delta_{i=p+r} - \delta_{p=r+i} - \delta_{r=i+p}$$

when $(X,Y,Z) = (C,C,S)$.

The wave-mean flow interaction coefficients are (with s as the meridional mode of the zonal flow):

$$c_{S(i,j)\,C(p,q)\,M(s)} = -c_{C(i,j)\,S(p,q)\,M(s)} = \frac{\sqrt{2}nps}{\pi}\left(\frac{1}{j+q-s} + \frac{1}{j-q+s} - \frac{1}{j+q+s} - \frac{1}{j-q-s}\right) \times \delta_{i=p}\delta_{j+q+s=\mathrm{odd}}, \tag{A4}$$

$$c'_{M(s)\,S(i,j)\,C(p,q)} = -c'_{M(s)\,C(i,j)\,S(p,q)} = \frac{\sqrt{2}nps}{\pi}\left(\frac{1}{j+q-s} + \frac{1}{j-q+s} + \frac{1}{j+q+s} + \frac{1}{j-q-s}\right) \times \delta_{i=p}\delta_{j+q+s=\mathrm{odd}}. \tag{A5}$$

The δ_g terms in these equations are simply resonance conditions to determine whether three different scales can interact with each other and are useful in analyzing the influence of model truncation on nonlinear interactions (see Subsection 5.1).

REFERENCES

Cehelsky, P. and Tung, K-K. 1987. Theories of multiple equilibria and weather regimes—a critical reexamination. Part II: baroclinic two-layer models. *J. Atmos. Sci. 44*, 3282–3303.

Charney, J. G. and Straus, D. M. 1980. Form-drag instability, multiple equilibria, and propagating planetary waves in baroclinic, orographically forced, planetary wave systems. *J. Atmos. Sci. 37*, 1157–1176.

Curry, J. H., Herring, J. R., Loncaric, J. and Orszag, S. A. 1984. Order and disorder in two- and three-dimensional Bénard convection. *J. Fluid Mech. 147*, 1–38.

Ebusizaki, W. 1988. Dynamical criterion for a marginally unstable, quasi-linear behavior in a two-layer model. *J. Atmos. Sci. 45*, 1721–1729.

Held, I. M. 1975. Momentum transport by quasi-geostrophic eddies. *J. Atmos. Sci. 32*, 1494–1499.

Held, I. M. 1978. The tropospheric lapse rate and climatic sensitivity: Experiments with a two-level atmospheric model. *J. Atmos. Sci. 35*, 2083–2098.

Held, I. M. and Suarez, M. J. 1978. A two-level primitive equation atmospheric model designed for climatic sensitivity experiments. *J. Atmos. Sci. 35*, 206–269.

Lorenz, E. 1971. N-cycle time differencing for stepwise numerical integration. *Mon. Weath. Rev. 99*, 644–648.

Newell, R. E., Kidson, J. W., Vincent, D. G. and Boer, G. J. 1972. *The general circulation of the tropical atmosphere and interactions with extratropical latitudes. Vol. 1*. Cambridge, Mass.: MIT Press, 258 pp.

O'Brien E. and Branscome, L. E. 1988. Modes of variability in a low-order two-level model. *Tellus 40A*, 358–374.

Oort, A. H. 1964. On estimates of the atmospheric energy cycle. *Mon. Weath. Rev. 92*, 483–493.

Oort, A. H. 1983. *Global atmospheric circulation statistics, 1958–1973*. NOAA Prof. Pap. 14. Washington, D.C.: US Dept. of Commerce, 180 pp.

Pedlosky, J. 1964. The stability of currents in the atmosphere and ocean: Part II. *J. Atmos. Sci. 21*, 342–353.

Phillips, N. A. 1956. The general circulation of the atmosphere: a numerical experiment. *Quart. J. R. Met. Soc. 82*, 123–164.

Reinhold, B. 1988. Structural determinism of equilibrated baroclinic waves in a two-layer model and equivalent barotropy. *Tellus 40A*, 375–391.

Reinhold, B. and Pierrehumbert, R. T. 1982. Dynamics of weather regimes: quasi-stationary waves and blocking. *Mon. Weath. Rev. 110*, 1105–1145.

Rhines, P. B. 1977. The dynamics of unsteady currents. In: *The sea, Vol. 6* (eds. E. A. Goldberg, I. N. McCane, J. J. O'Brien and J. H. Steele). New York: Wiley, 189–318.

Salmon, R. L. 1980. Baroclinic instability and geostrophic turbulence. *Geophys. Astrophys. Fluid Dyn. 15*, 167–211.

Stone, P. H. 1972. A simplified radiative-dynamical model for the static stability of rotating atmospheres. *J. Atmos. Sci. 29*, 405–418.

Stone, P. H. 1978. Baroclinic adjustment. *J. Atmos. Sci. 35*, 561–571.

Tung, K-K. and Rosenthal, A. J. 1987. Low-frequency nonlinear dynamics of quasi-geostrophic waves in a midlatitude channel and the effects of tropical influence. *J. Atmos. Sci. 44*, 3821–3826.

Vallis, G. K. 1983. On the predictability of quasi-geostrophic flow: the effects of beta and baroclinicity. *J. Atmos. Sci. 40*, 10–27.

Vallis, G. K. 1988. Numerical studies of eddy transport properties in eddy-resolving and parametrized models. *Quart. J. Roy. Meteor. Soc. 114*, 183–204.

Wiin-Nielsen, A. 1968. On the intensity of the general circulation of the atmosphere. *Rev. Geophys. 6*, 559–579.

Yoden, S. 1983. Nonlinear interactions in a two-layer, quasi-geostrophic low-order model with topography. Part I: Zonal flow-forced wave interactions. *J. Met. Soc. Japan 61*, 1–18.